JOURNAL OF CHEMICAL INFORMATION AND MODELING

Article

pubs.acs.org/jcim

Bridging Molecular Docking to Membrane Molecular Dynamics To Investigate GPCR–Ligand Recognition: The Human A_{2A} Adenosine Receptor as a Key Study

Davide Sabbadin, Antonella Ciancetta, and Stefano Moro*

Molecular Modeling Section (MMS), Dipartimento di Scienze del Farmaco, Università di Padova, via Marzolo 5, 35131 Padova, Italy

Supporting Information

ABSTRACT: G protein-coupled receptors (GPCRs) represent the largest family of cell-surface receptors and about one-third of the actual targets of clinically used drugs. Following the progress made in the field of GPCRs structural determination, docking-based screening for novel potent and selective ligands is becoming an increasingly adopted strategy in the drug discovery process. However, this methodology is not yet able to anticipate the "bioactive" binding mode and discern it among other conformations. In the present work, we present a novel approach consisting in the integration of molecular docking and membrane MD simulations with the aim to merge the rapid sampling of ligand poses into in the binding site, typical of docking algorithms, with the thermodynamic accuracy of MD simulations in describing, at the molecular level, the stability a GPCR-ligand complex embedded into explicit lipid–water environment. To validate our approach, we have chosen as a key study the human A_{2A} adenosine receptor (hA_{2A} AR) and selected four receptor–antagonist complexes and one receptor–agonist complex that have been recently crystallized. In light of the obtained results, we believe that our novel strategy can be extended to other GPCRs and might represent a valuable tool to anticipate the "bioactive" conformation of high-affinity ligands.

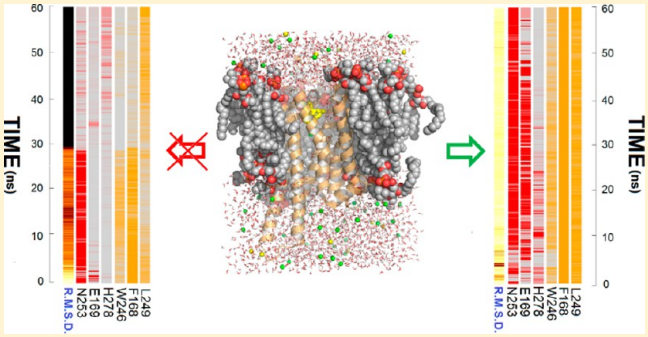

INTRODUCTION

G protein-coupled receptors (GPCRs) are the largest family of cell-surface receptors and represent ~3% of the genes in the human genome.[1] They regulate several crucial functions of most cells in the body, and receptor dysfunction can lead to a variety of disease conditions.[2] These receptors respond to a wide variety of structurally diverse ligands, ranging from small molecules (such as biogenic amines, nucleotides, and ions) to lipids, peptides, proteins, and even light.[3] Ligands (agonists, inverse agonists, and antagonists) acting on GPCRs play an important role in the treatment of numerous diseases, including cardiovascular and mental disorders, cancer, and viral infections.[2] It is estimated that these receptors represent about one-third of the actual identified targets of clinically used drugs.[4,5] The determination of the rhodopsin crystal structure and, more recently, adrenergic, dopaminergic, histaminergic, opioid and A_{2A} adenosine receptors provides both academia and pharma companies with exceptionally valuable information for a better understanding of the molecular determinants of receptor function and a more-reliable rationale for drug design.[6]

The progress made in the field of GPCRs structural determination has increased the adoption of docking-based screening for novel potent and selective ligands with a potentially significant savings of time and money. However, despite many advances carried out in the molecular docking field during the past decade, this methodology is still far from being realistic and accurate.[7] More commonly, the goodness of chemical complementarity between the ligand and its receptor is evaluated by an energy function (*scoring function*) composed of different energetic terms that attempt to account for the *forces driving* ligand *binding* to the receptor.[8] As recently demonstrated, docking programs are usually successful in generating multiple poses that include binding modes similar to the crystallographically determined bound structure, whereas scoring functions are much less successful at correctly identifying the "bioactive" binding mode.[7] This narrows the applicability of the methodology to those cases where the crystallographic structure is available for comparison and generally implies the need for the calibration of the docking protocol through benchmark studies.

However, to date, only ~1% of GPCRs structures has been experimentally determined with the consequence that the research focused on the majority of the targets of interest is based on structures obtained by homology modeling. Therefore, novel approaches are needed to increase docking robustness and applicability, not only to anticipate the "bioactive" pose of a ligand within the receptor crystallographic structure but also to discriminate true binders from an ensemble of decoys.

Received: September 23, 2013
Published: December 20, 2013

dx.doi.org/10.1021/ci400532b | J. Chem. Inf. Model. 2014, 54, 169–183

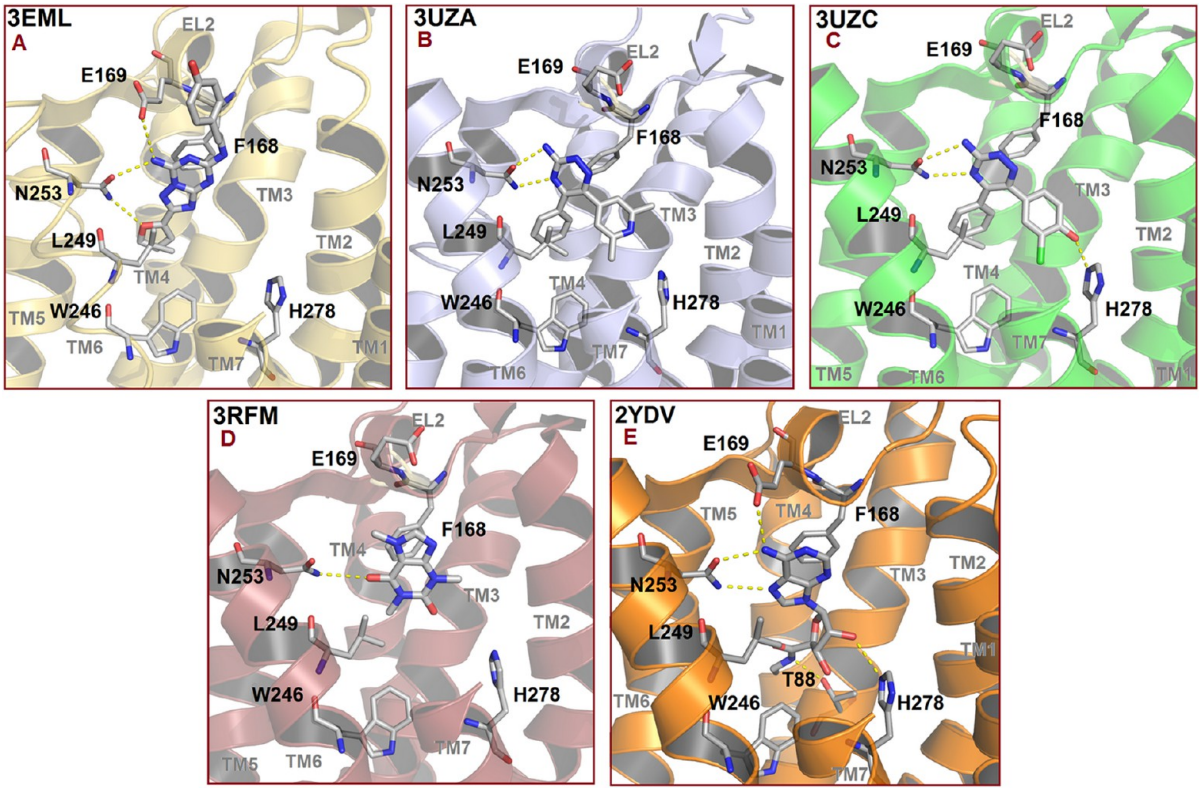

Figure 1. Overview of the binding modes at the hA_{2A} AR of the selected co-crystallized ligands: (A) ZM 241385 (PDB ID: 3EML), (B) T4G (PDB ID: 3UZA), (C) T4E (PDB ID: 3UZC), (D) caffeine (PDB ID: 3RFM), and (E) NECA (PDB ID: 2YDV). The complexes are viewed from the membrane side facing TM6 and TM7, with the view of TM7 partially omitted. Side chains of the amino acids crucial for ligand binding are displayed as gray sticks. Hydrogen atoms are not displayed, whereas hydrogen bond interactions are highlighted as yellow dashed lines.

Very recently, sophisticated molecular dynamics (MD) approaches adapted to massively parallel computer architectures have allowed the execution of microsecond-scale standard MD simulations of fully atomistic representations of GPCRs embedded into explicit lipid−water environments.[9] Unfortunately, although MD simulations represent the highly accurate modeling methods dealing with macromolecular systems, they still remain computationally expensive and require costly high-performance computing (HPC) resources.[10] The recent evolution of commodity graphics processing units (GPUs) represents an important technological innovation that may realize the full potential of atomistic molecular modeling and simulation.[11] In fact, the ability to rapidly compute realistic estimates of binding energies would be of great use in drug discovery process in particular as a robust alternative to the conventional scoring functions in molecular docking field. However, the exact thermodynamic methods using MD require long-running simulations, thus making the total computation time uncompetitive with direct experimental measurements. To be a practical complement to the experimental techniques, a computational method must have a time-to-answer on the order of a few days. Interestingly, GPUs can currently deliver more floating-point operations per second (FLOPS) (by more than an order of magnitude) than standard processors, thereby also drastically reducing the computational time cost of long-term fully atomistic MD simulations.[11]

In the present work, we present a novel approach consisting in the integration of molecular docking and membrane MD simulations with the aim to merge the main advantage of docking, that is the rapid sampling of ligand poses into the binding site, with the thermodynamic accuracy of MD simulations in particular regarding the description, at the molecular level, of the stability a GPCR−ligand complex embedded into explicit lipid−water environment. In other words, we would like to verify if the "energy inspection" of membrane MD trajectory obtained starting from different GPCR−ligand docking poses may improve our ability to identify the "bioactive" pose of a ligand within the receptor crystallographic structure. This would allow us to overcome some of the most crucial "energy-related" approximations of the conventional scoring functions, such as the absence of explicit water molecules and the exploration of the GPCR-ligand complex flexibility. In particular, all membrane MD simulations have been carried out using an ACEMD program engineered to run on GPUs.[12]

To validate our combined approach, we have selected, as a key study, the human A_{2A} adenosine receptor (hA_{2A} AR), which has been recently crystallized with several ligands, both agonists and antagonists, characterized by different receptor binding affinities. In particular, we have focused our attention on hA_{2A} AR antagonists since they are gaining interest because of their potential use for the treatment of a variety of neurological disorders, such as Parkinson's disease, Huntington's disease, and migraines.[13] Recently, phase III studies on Preladenant, which is an A_{2A} AR antagonist, as a potential drug for the treatment of Parkinson's disease were abandoned thus proving the need for concrete approaches that are able to improve the quality of GPCRs−ligand models for docking and screening applications and enable a detailed structural investigation of GPCRs−ligand interaction, by taking into account the role of water molecules in ligand binding as well as the influence of the membrane on protein flexibility.

dx.doi.org/10.1021/ci400532b | J. Chem. Inf. Model. 2014, 54, 169−183

For the present study, we have selected five crystal structures of the hA_{2A} AR in complex with four strong binders, such as 4-(2-(7-amino-2-(2-furyl)(1,2,4)triazolo(2,3-*a*)(1,3,5)triazin-5-yl-amino)ethyl)phenol, ZM 241385 (pK_D = 9.18 ± 0.00,[14] Protein DataBank (PDB) ID: 3EML[15]); 6-(2,6-dimethylpyridin-4-yl)-5-phenyl-1,2,4-triazin-3-amine, T4G (pK_D = 8.9 ± n.d.,[14] PDB ID: 3UZA[16]); 4-(3-amino-5-phenyl-1,2,4-triazin-6-yl)-2-chlorophenol, T4E (pK_D = 9.6 ± n.d.,[14] PDB ID: 3UZC[16]); NECA, *N*-ethyl-5′-carboxamido adenosine (pK_D = 7.00 ± 0.1,[14] PDB ID: 2YDV[17]) and a weaker binder such as caffeine (pK_D = 5.31 ± 0.44,[14] PDB ID: 3RFM[14]). The structures of the considered antagonists inside the orthosteric binding pocket of the hA_{2A} AR are collected in Figure 1. The obtained results prove that the strategy is able to reproduce the "bioactive" conformation of high affinity ligands and to discern it among other "less stable" conformations, as described in details in the following.

METHODS

Computational Facilities. All computations were performed on a hybrid CPU/GPU cluster. In particular, molecular docking simulations have been carried out using 8 Intel Xeon E5620 CPU cluster, whereas membrane molecular dynamics simulation have been performed with a 4 NVIDIA GTX 580 and 2 NVIDIA GTX 680 GPU cluster engineered by Acellera.[18]

In the following, the numbering of the amino acids follows the arbitrary scheme by Ballesteros and Weinstein: each amino acid identifier starts with the helix number, followed by the position relative to a reference residue among the most conserved amino acids in that helix, to which the number 50 is arbitrarily assigned.[19]

Homology Models. The selected five crystal structures (PDB IDs: 3EML, 3UZA, 3UZC, 3RFM, and 2YDV) and the FASTA sequence of the hA_{2A} AR (Uniprot ID: P29274) were retrieved from the RCSB PDB database[20] (http://www.rcsb.org) and the UniProtKB/Swiss-Prot,[21−23] respectively. The eventual lysozyme portion fused to the receptor, as well as co-crystallized ligands and water molecules, have been removed before starting the homology modeling procedure. Ionization states and hydrogen positions have been assigned with the "Protonate-3D" tools.[24] Then, to minimize contacts among hydrogens, the structures were subjected to energy minimization with Amber99 force field[25] until the root-mean-square (RMS) of the conjugate gradient was <0.05 kcal mol^{-1} $Å^{-1}$, by keeping the heavy atoms fixed at their crystallographic positions. The FASTA sequence was aligned, using Blosum 62 matrix, with the template sequence. Backbone and conserved residues coordinates were copied from the template structure, whereas newly modeled regions and nonconserved residues side chains were modeled and energetically optimized using an Amber99 force field until a RMS of the conjugate gradient of <0.05 kcal mol^{-1} $Å^{-1}$ was reached. Missing loop domains were constructed by the loop search method implemented in the Molecular Operating Environment (MOE, version 2010.10) program,[26] on the basis of the structure of compatible fragments found in the PDB.[20] N-terminal and C-terminal were deleted if their lengths exceeded those found in the crystallographic template. The "Protonate-3D" tool was used to appropriately assign ionization states and hydrogen positions[24] to the build models. Protein stereochemistry evaluation was then performed by employing several tools (Ramachandran and χ plots measure j/ψ and χ_1/χ_2 angles, clash contacts reports) implemented in the MOE suite.[26]

Docking. Co-crystallized agonist and antagonists structures were extracted from the original protein−ligand complex coordinates files and checked for errors. Hydrogen atoms were added and the protonation state (pH 7.4) was checked. Partial charges for ligands were imported from the MOPAC program output files using the PM3/ESP semiempirical Hamiltonian,[27,28] whereas partial charges for protein amino acids were calculated on the basis of the Amber99 force field. Ligands were docked into the orthosteric binding site of the hA_{2A} AR models with the GOLD 5.1 suite using the genetic algorithm protocol[29] (10 independent docking runs for each compound) and the CHEMPLP scoring function. The outcoming poses have been then rescored on the basis of the GoldScore scoring function.[29,30] The latter, in a previous study,[31] resulted the best among the tested scoring functions in reproducing and ranking the crystallographic binding mode of ZM 241385 at the hA_{2A} AR.[32] The purpose of the docking procedure was to use the search algorithm to identify as many different binding modes as possible: we therefore forced the program to retain 10 poses that differed in terms of the root-mean-square deviation (RMSD) for at least 1.75 Å, by setting the non default "diverse solutions" keyword, as implemented in the GOLD suite. The resulting conformations have been sorted according to the cluster number. The values of the Fitness Score, as evaluated by the GoldScore scoring functions, and the RMSD values with respect to the corresponding crystal structures are reported in Table S1 in the Supporting Information.

Interaction Energy Fingerprints (IEFs). To analyze the ligand−receptor recognition mechanism in a more quantitative manner, we calculated the individual electrostatic and hydrophobic contributions to the interaction energy (hereby denoted as IE_{ele} and IE_{hyd}, respectively) of each receptor residue involved in the binding with the ligand. In particular, the electrostatic contribution has been computed on the basis of the nonbonded electrostatic interaction energy term of the force field,[33] whereas the hydrophobic contributions has been calculated by using the directional hydrophobic interaction term based on contact surfaces as implemented in the MOE scoring function.[26] As a consequence, an energy (expressed in units of kcal mol^{-1}) is associated to the electrostatic contribution, whereas a score (the higher the better) is related to the hydrophobic contribution.

The analysis of these contributions have been reported as "interaction energy fingerprints" (hereby indicated as IEFs), i.e., interaction energy patterns (graphically displayed either as histograms or as heatlike maps) reporting the key residues involved in the binding with the considered ligands along with a quantitative estimate of the occurring interactions.

Molecular Dynamics. Each ligand−receptor complex was embedded in a 1-palmitoyl-2-oleoyl-sn-glycero-3-phosphocholine (POPC) lipid bilayer (75 Å × 75 Å wide) and placed into the membrane according to the suggested orientation reported in the "Orientations of Proteins in Membranes (OPM)" database[34] for the hA_{2A} AR in complex with the antagonist T4G (PDB ID: 3UZA[16]). The membrane has been generated by using a grid-based method[35] with the VMD Membrane Plugin tool[36] and overlapping lipids (within 0.6 Å) were removed upon insertion of the protein. The total number of lipids composing the lipid bilayer of each considered membrane-embedded ligand−protein system are reported in Table S2 in the Supporting Information (upper panel), whereas a detailed

dx.doi.org/10.1021/ci400532b | J. Chem. Inf. Model. 2014, 54, 169−183

representation is depicted in Figure S2 in the Supporting Information (panel I).

The prepared systems were solvated with TIP3P[37] water using the Solvate 1.0 program[38] and neutralized by Na^+/Cl^- counterions to a final concentration of 0.154 M. The total number of atoms per system was ~35 000. Membrane MD simulations were carried out on a GPU cluster with the ACEMD program,[12] using the CHARMM27 Force Field[33] and periodic boundary conditions. Initial parameters for the ligands were derived from the CHARMM General Force Field for organic molecules,[39] using the "paramchem" service,[40,41] and were subsequently optimized at the MP2/6-31G* level of theory[42] (which is consistent with the CHARMM27 Force Field parametrization) using Gaussian 09[43] and the implemented parametrization tools in the VMD engine.[36]

The system was equilibrated using a stepwise procedure. In the first stage, to reduce steric clashes due to the manual setting up of the membrane-receptor system, a 500-step conjugate-gradient minimization was performed. Then, to allow lipids to reach equilibrium and water molecules to diffuse into the protein cavity, the system was equilibrated by keeping the positions of protein and ligand atoms restrained for the first 8 ns, using a force constant of 1 kcal mol^{-1} $Å^{-2}$ and then by keeping only the α carbon atoms frozen up to 9 ns while gradually reducing the force constant to 0.1 kcal mol^{-1} $Å^{-2}$. During the equilibration procedure, the temperature was maintained at 298 K, using a Langevin thermostat with a low damping constant of 1 ps^{-1}, and the pressure was maintained at 1 atm using a Berendensen barostat. Bond lengths involving hydrogen atoms were constrained using the M-SHAKE[44] algorithm with an integration time step of 2 fs.

In order to assess the biophysical validity of the built systems, the average area per lipid headgroup (APL) and bilayer thickness measurements for each built system was measured using Grid-MAT-MD.[45] The corresponding averaged area per lipid headgroup of the extracellular leaflet (eAPL) and of the intracellular leaflet (iAPL) in the first nanosecond (eAPL1 ns and iAPL1 ns) and in the last nanosecond (eAPL9 ns and iAPL9 ns) of the equilibration for all the considered complexes is reported in Table S2 in the Supporting Information (lower panel). The calculated values are in agreement with the experimental values measured for 1-palmitoyl-2-oleoyl-sn-glycero-3-phosphocholine (POPC) lipid bilayers.[46] Bilayer system representation and the performed thickness analysis, for each built system at the end of the equilibration phase, are reported in Figure S2 in the Supporting Information (panels I and II, respectively). Harmonical constraints were then removed during an additional 60 ns (NVT ensemble). Long-range Coulomb interactions were handled using the particle mesh Ewald summation method (PME)[47] with grid size rounded to the approximate integer value of cell wall dimensions. A nonbonded cutoff distance of 9 Å with a switching distance of 7.5 Å was used.

The total of 69 ns of membrane molecular dynamics took ~45 h of NVIDIA GTX580 GPU time per trajectory. All molecular dynamics experiments were carried out in triplicate for a total of ~10 μs of MD trajectories that resulted in ~1100 h per single GPU used.

Dynamic Scoring Function. The dynamic scoring function (DSF) is defined as the cumulative sum of the electrostatic (IE_{ele}) and hydrophobic (IE_{hyd}) contributions to ligand binding during the MD trajectories computed at frames extracted every 100 ps. To calculate such contributions, dynamic selections of residues within a range of 4.5 Å from the ligand have been selected for the calculation of the electrostatic DSF (DSF_{ele}, eq 1) and the hydrophobic DSF (DSF_{hyd}, eq 2):

$$DSF_{ele} = \sum_{t=0}^{n} IE_{ele} \quad (1)$$

$$DSF_{hyd} = \sum_{t=0}^{n} IE_{hyd} \quad (2)$$

Moreover, to take into account the degree of fitness of the predicted binding conformations and to highlight differences between stable and unstable poses, we also calculated the value of the weighted DSF (wDSF) by dividing the values in eqs 1 and 2 by the ligand fluctuation (RMSD), with respect to the starting position generated by the docking protocol. The corresponding weighted electrostatic and hydrophobic DSFs (denoted as $wDSF_{ele}$ and $wDSF_{hyd}$, respectively) are reported in eqs 3 and 4:

$$wDSF_{ele} = \frac{\sum_{t=0}^{n} IE_{ele}}{RMSD} \quad (3)$$

$$wDSF_{hyd} = \frac{\sum_{t=0}^{n} IE_{hyd}}{RMSD} \quad (4)$$

The obtained DSF and wDSF values then were plotted against the simulation time and generic linear functions ($f(x) = m{\cdot}x$) were fitted to the collected data. The slope coefficients of the fitted lines provide an estimate of the enduring strength of the interaction with the nearby residues, thus highlighting differences between stable and unstable binding modes: Higher slope coefficients (absolute value) are associated with ligand conformations that are strongly and steadily bound to the residues, whereas lower slope values correspond to ligand conformations that possess a low degree of fitness with the binding pocket and are expected to differ from the "bioactive" conformation. Slope coefficients are reported in Table S3 in the Supporting Information.

Multimedia Materials. Trajectory analysis and the generation of figures and videos were performed using several functionalities implemented in VMD,[36] the PyMOL Molecular Graphics System, Version 1.5.0.4 Schrödinger, LLC, and a Gnuplot graphic utility (http://www.gnuplot.info/).

RESULTS AND DISCUSSION

General Features of the Orthosteric Binding Site of the hA_{2A} AR. The binding site of the hA_{2A} AR has been exhaustively described elsewhere.[6] Therefore, here, we report the most relevant receptor−ligand binding features that we have taken into account to inspect and analyze the results of molecular docking and MD simulations. As depicted in Figure 1, the common interaction pattern for all ligands involves an aromatic $\pi-\pi$ stacking with the conserved Phe168, located in the second extracellular loop (EL2), and additional hydrophobic contacts with, among others, the Leu249 (6.51) side chain. Strong polar interactions are established with the side chain of the conserved Asn253 (6.55),[48] where the role of the hydrogen bond donor in the high-affinity ligands is played by an exocyclic amine group. In the structure co-crystallized with ZM 241385 (Figure 1A), the side chain of Glu169 (EL2) is involved in an additional hydrogen bond, whereas in the other

dx.doi.org/10.1021/ci400532b | J. Chem. Inf. Model. 2014, 54, 169−183

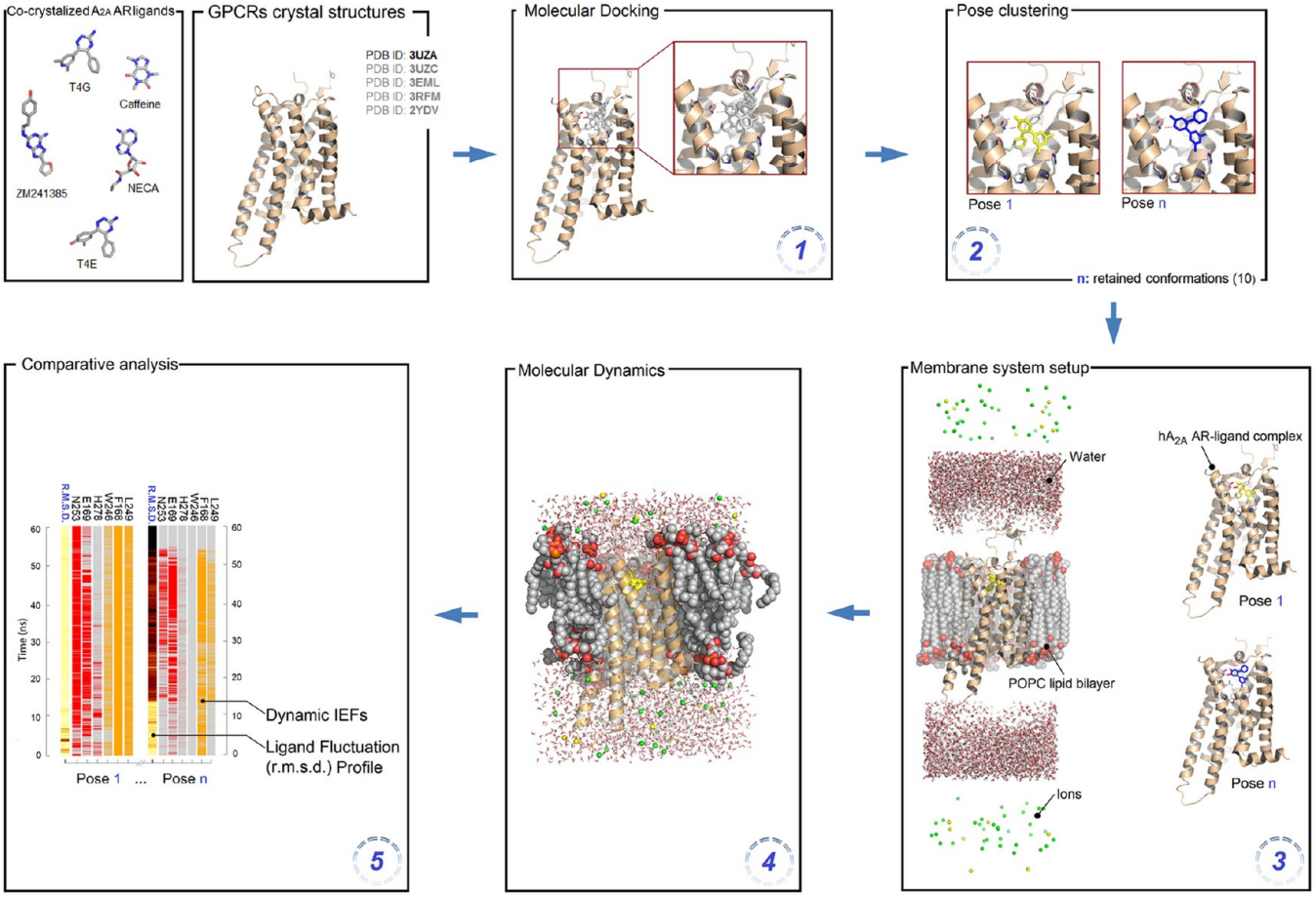

Figure 2. Workflow of the combined molecular docking and membrane molecular dynamics protocol.

structures, the residue is found in a different rotameric state, preventing such interaction. Moreover, in the agonist-bound crystal structure, the Thr88 (3.36) side chain forms a hydrogen bond interaction with the nitrogen atom of the acetamide moiety in NECA. This pattern is consistent with the previously reported mutation data, which have been recently reviewed by Crystalli and collaborators,[49] showing a loss of affinity for the Asn253 (6.55) mutant, as well as with recent mutagenesis data,[48] revealing the critical role of Phe168 (EL2) and Leu249 (6.51) for both agonists and antagonists binding and of Thr88 (3.36) for agonist binding.

Workflow of the Combined Molecular Docking and Membrane MD Protocol. As anticipated in the Introduction, one of the most difficult tasks in structure-based drug discovery is the accurate prediction of receptor−ligand binding interactions. For this purpose, molecular docking and scoring functions are the most used approaches. However, often, the top-ranked docking poses do not represent the "bioactive" (crystallographic) binding mode, and very frequently, there is no correlation between docking scores and binding affinity data.[50,51] Therefore, the "post-processing" of docking poses has recently emerged as a strategy to raise the success of docking studies and several approaches have been proposed.[52] In this work, we present an alternative method consisting in the integration of molecular docking and membrane MD simulations with the aim to merge the main advantage of docking, that is the rapid sampling of ligand poses into in the binding site, with the thermodynamic accuracy of MD simulations in particular regarding the description, at the molecular level, of the stability a GPCR-ligand complex embedded into explicit lipid−water environment. The workflow of the combined protocol is shown in Figure 2: Starting from a conventional receptor-driven docking protocol, the top 10 ranked poses have been clustered (clustering distance = 1.75 Å) and each pose-receptor complex was embedded in a 1-palmitoyl-2-oleoyl-sn-glycero-3-phosphocholine (POPC) lipid bilayer and subjected to 60 ns of MD simulations (in triplicate). From the resulting MD trajectories, we analyzed in details the following three aspects: (i) the evolution of the IEFs (the hereby denoted as "dynamic IEFs") that highlights if the interaction of the ligands with the surrounding residues is conserved throughout the considered time lapse, (ii) the ligand fluctuation profile (expressed in terms of RMSD) that reflects the "positional stability" of the starting conformation, and (iii) the cumulative sum of ligand receptor interactions that provides a dynamic estimate of both the positional stability and the strength of the interaction network. Indeed, as in principle, the "bioactive" (crystallographic) binding mode is the one in which an high-affinity ligand is strongly anchored to its orthosteric binding site, it is expected that the docking pose that better reproduces it shows both a stable position and a persistent interaction network during the simulations. To validate our protocol, we have selected five crystal structures of the hA_{2A} AR in complex with four strong binders such as ZM 241385 (PDB ID: 3EML), T4G (PDB ID: 3UZA), T4E (PDB ID: 3UZC), NECA (PDB ID: 2YDV), and the weaker binder caffeine (PDB ID: 3RFM).

dx.doi.org/10.1021/ci400532b | J. Chem. Inf. Model. 2014, 54, 169−183

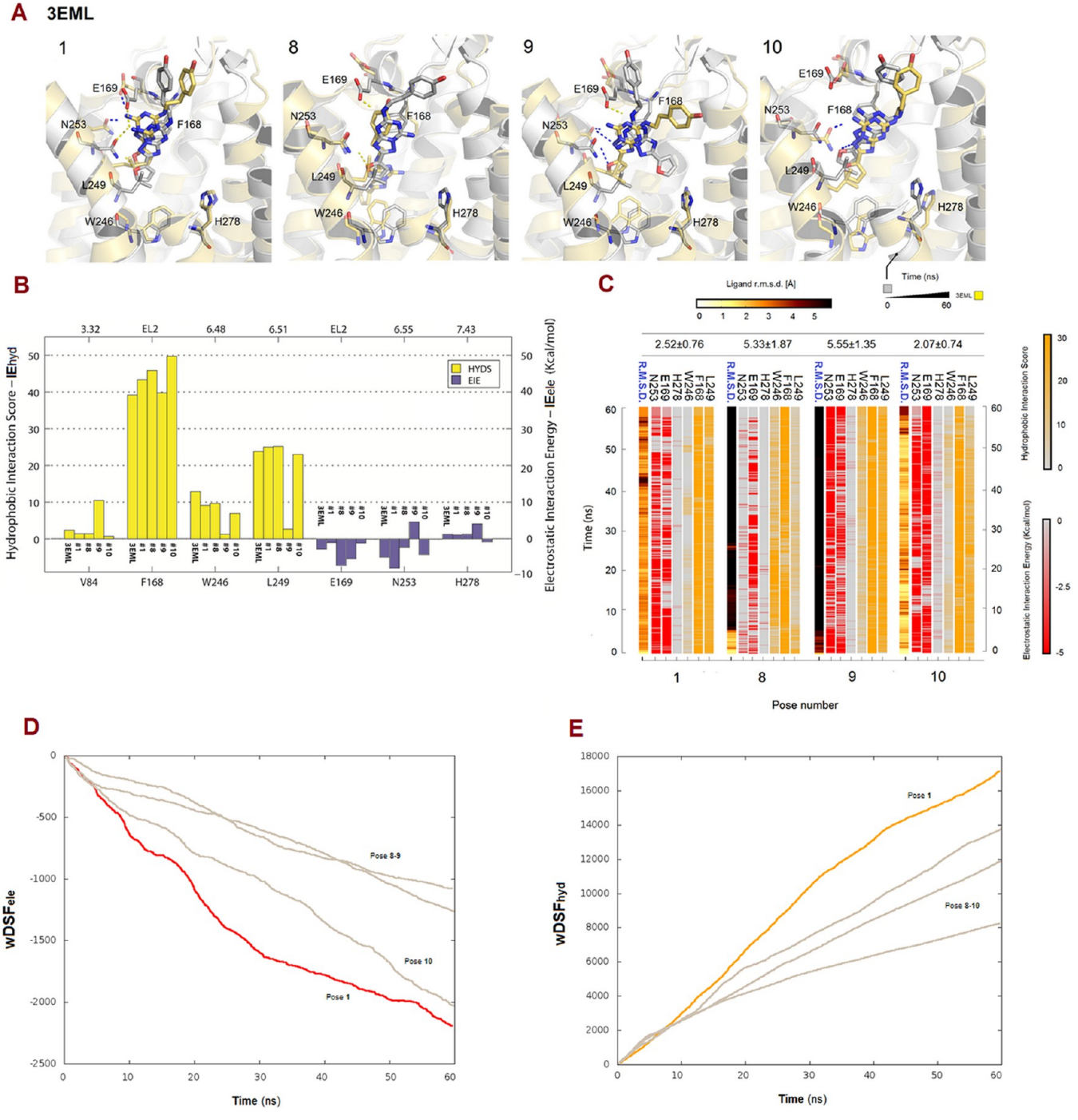

Figure 3. (A) Docking poses of ZM 241385 at the hA_{2A} AR with their corresponding (B) static IEFs and (C) dynamic IEFs, and (D) electrostatic wDSFs and (E) hydrophobic wDSFs. IE_{ele} values are given in units of kcal $Å^{-1}$ mol^{-1}, IE_{hyd} values are given in arbitrary hydrophobic units, and ligand fluctuations (average RMSD reported on top of the IEFs) are given in Å.

In Silico Inspection of ZM 241385 Binding Mode. We first tested our combined procedure with the potent hA_{2A} AR antagonist ZM 241385: In the majority of the retained docking poses (poses 1−7), the aromatic core is superimposed (poses 1−7: RMSD < 1 Å; see Table S1 in the Supporting Information and Figure 3A) to the corresponding co-crystallized ligand and the observed interaction patterns reflect the same key interactions highlighted by the crystallographic structure[15] (Figure 3B).

Membrane MD simulation of pose 1 (see Figure 3A, as well as Table S1 in the Supporting Information) is characterized by a high positional stability (RMSD = 2.52 ± 0.76 Å) and the analysis of dynamical IEFs (see Figure 3C) reveals strong and persistent interactions with Asn253 (6.55), Glu169 (EL2), Phe168 (EL2), and Leu249 (6.51). Similar results have been obtained from the MD simulations of all of the other seven ligand-protein complexes (poses 2−7, data not shown). Although the IEFs pattern of pose 8 (Figure 3B) apparently mirrors that observed for the co-crystallized structure, the ligand has a different orientation into the binding pocket. Indeed, the exocyclic amino group points toward TM2 and does not interact with any residue within a range of 4.5 Å, and

dx.doi.org/10.1021/ci400532b | J. Chem. Inf. Model. 2014, 54, 169−183

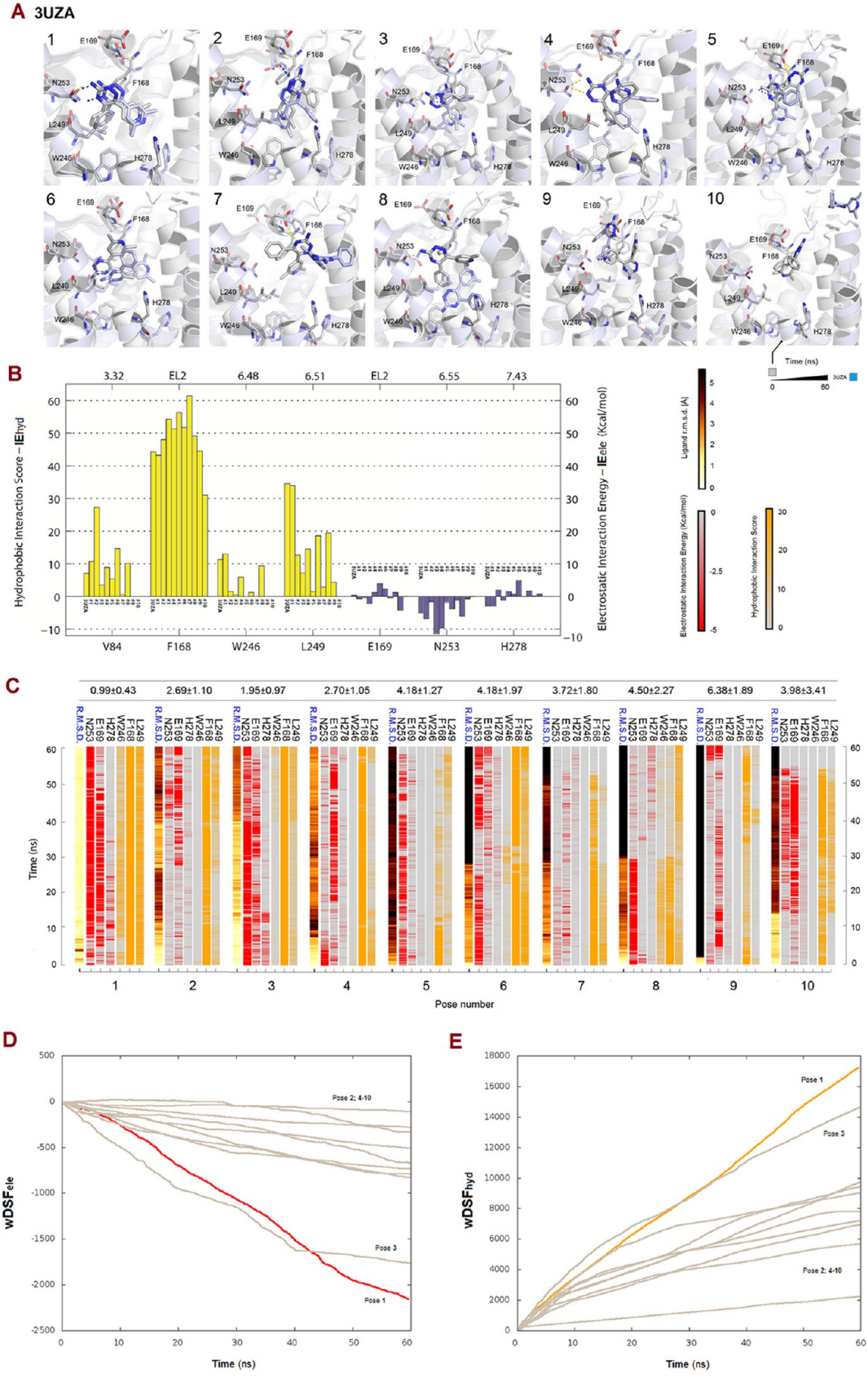

Figure 4. (A) Docking poses of T4G at the hA_{2A} AR with their corresponding (B) static IEFs and (C) dynamic IEFs, and (D) electrostatic wDSFs and (E) hydrophobic wDSFs. IE_{ele} values are given in units of kcal $Å^{-1}$ mol^{-1}, IE_{hyd} values are given in arbitrary hydrophobic units, and ligand fluctuations (average RMSD reported on top of the IEFs) are given in Å.

dx.doi.org/10.1021/ci400532b | J. Chem. Inf. Model. 2014, 54, 169−183

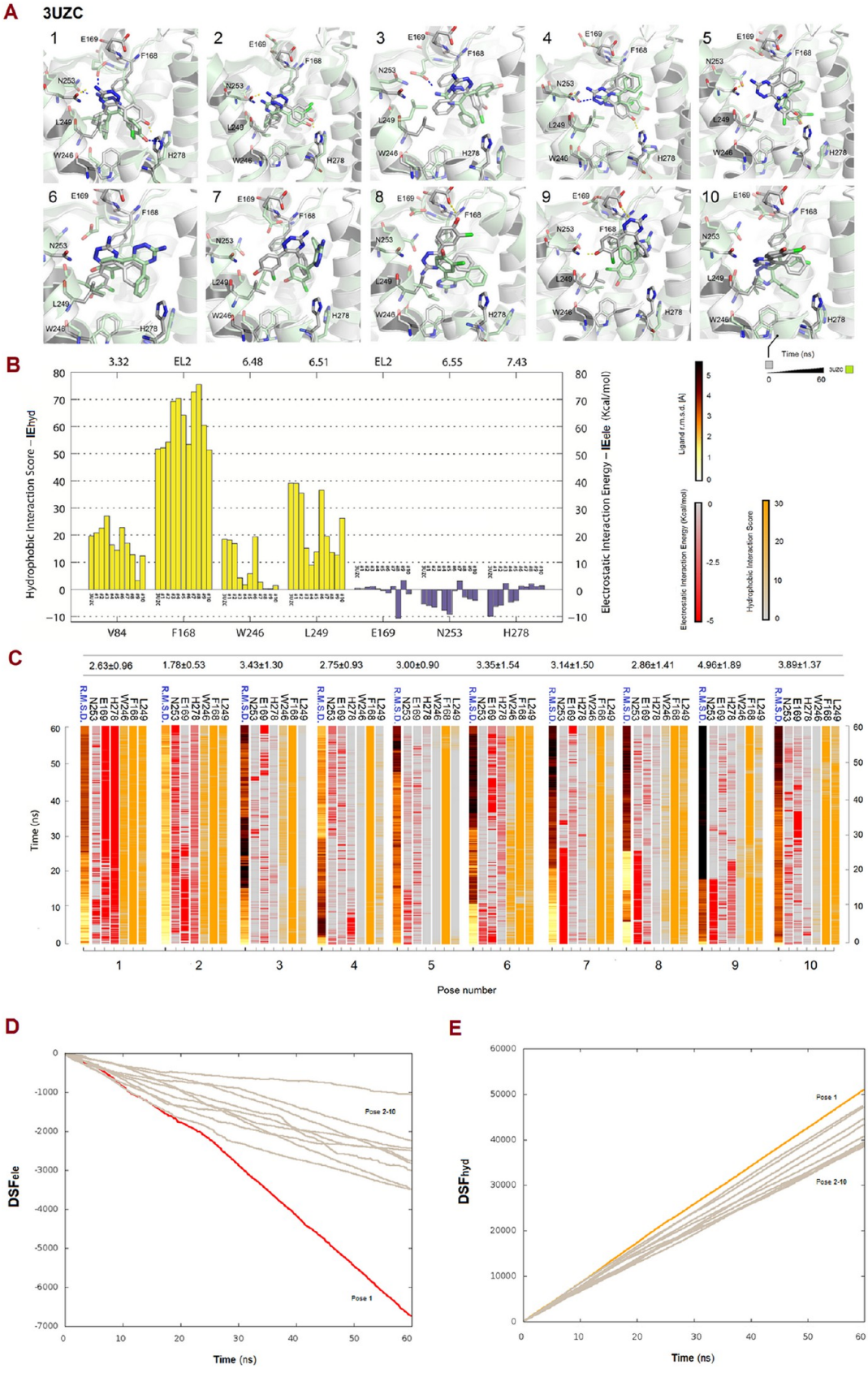

Figure 5. (A) Docking poses of T4E at the hA_{2A} AR with their corresponding (B) static IEFs and (C) dynamic IEFs, and (D) electrostatic DSFs and (E) hydrophobic DSFs. IE_{ele} values are given in kcal/mol, IE_{hyd} values are given in arbitrary hydrophobic units, and ligand fluctuations (average RMSD reported on top of the IEFs) are given in Å.

dx.doi.org/10.1021/ci400532b | J. Chem. Inf. Model. 2014, 54, 169−183

the polar interactions with Asn253 and Glu169 are established by the nitrogen atom in the triazole ring and the aminoethyl moiety, respectively (see Figures 3A and 3B). During the MD simulation (Figure 3C), these initially predicted strong hydrogen bonds are lost and the high average RMSD value (5.33 ± 1.87 Å) further confirms the low degree of fitness of the starting pose. Conversely, although poses 9 and 10 also exhibit a different initial orientation of the scaffold, with respect to the co-crystallized ligand (RMSD: 3.58 and 2.47 Å, respectively), during the MD simulation both poses are able to establish strong polar interactions with Asn253 (6.55) and Glu169 (EL2) (see Figures 3A and 3C).

Moreover, as reported in Table S3 in the Supporting Information and graphically displayed in Figures 3D and 3E, the slope coefficients fitted on the DSFs and wDSFs highlight that the conformations that are nearly superimposable to the crystallographic information (pose 1) or whose evolution, during the MD simulation, converge to the crystallographic conformation[15] (pose 10) have the more favorable slope absolute values.

These results suggest new insights into the late recognition process of ZM 241385 at the hA_{2A} AR, an aspect which has been extensively and uniquely described for the β_2-adrenergic receptor.[9] The existence of possible meta-binding conformations, identified by poses 9 and 10 (Figure 3A), enriches the description of the events that might occur once the ligand has entered the binding cavity. More studies (e.g., by employing nonequilibrium MD methods such as steered MD) are needed to better assess the statistical probability of these events and to clarify the role of small energy barriers among different ZM 241385 binding conformations, recently detected by X-ray crystallography.[14]

In Silico Inspection of T4G Binding Mode. The conformations of T4G (Figure 4A) inside the orthosteric binding site of the hA_{2A} AR have RMSD values, with respect to the crystallographic structure, that span from 0.69 Å (pose 1, see Table S1 in the Supporting Information) to 7.72 Å (pose 10, see Table S1 in the Supporting Information). The variability of the conformations is also reflected by the corresponding IEFs, as depicted in Figure 4B.

Pose 1 (Figure 4A) shows an interaction pattern involving residues that play a critical role in antagonist recognition (Figure 4B): Both the endocyclic and exocyclic nitrogen atoms of the aromatic scaffold establish hydrogen bonds with Asn253 (6.55). The 5-phenyl ring is directed toward the conserved His250 (6.52) and Trp246 (6.48) residues and interacts with the hydrophobic side chain of Val84 (3.32). A $\pi-\pi$ stacking interaction occurs between the conserved Phe168 (EL2) side chain and the 1,2,4-triazine aromatic core, which additionally interacts with Leu249 (6.51). During the MD simulation (Figure 4C), the polar contacts with Asn253 (6.55) are maintained strong and persistent. Interestingly, Glu169 (EL2), which is not initially involved in any interaction with the ligand (Figure 4B), is recruited during the simulation and establishes an hydrogen bond with the exocyclic nitrogen atom (Figure 4A). The dynamic IEFs (Figure 4C) also highlight favorable and persistent hydrophobic contacts with Leu249 (6.51), Phe168 (EL2), and Trp246 (6.48). The stability of the initial binding mode is also confirmed by the low ligand fluctuation (average RMSD = 0.99 ± 0.43 Å). Again, also in the case of T4G, among the other poses, there are some whose interaction patterns share common features with the co-crystallized ligand (poses 3, 4, 5, 7, and 8) and others that do not establish polar interactions with key residues involved in antagonist recognition (poses 2, 6, 9, and 10). In all these cases, the MD simulations (Figure 4C) have revealed unstable interaction patterns and a low positional stability with a consistent increase of ligand fluctuations into the binding site.

This scenario is further confirmed by the analysis of the DSFs (Figures 4D and 4E) and their corresponding slope coefficients (Table S3 in the Supporting Information): The higher slope correspond to pose 1, whereas lower slopes are associated to the other possible binding conformations. The difference can be graphically detected in Figures 4D and 4E.

In Silico Inspection of T4E Binding Mode. As for T4G, also the docking poses for T4E (Figure 5A) show a variable range of superimposition with respect to the crystallographic structure ranging from 0.33 Å to 6.58 Å (Table S1 in the Supporting Information) with associated docking scores comprising bad placements (pose 10) as well as poses to which a high score is assigned (poses 1 and 2).

Pose 1 (Figure 5A) exhibits the most crucial ligand–receptor interactions observed for the co-crystallized ligand (Figure 5B). During the MD simulation, Asn253 (6.55) and His278 (7.43) play a major role in the ligand binding process (Figure 5C) and, interestingly, Glu169 is recruited from EL2, forming an additional polar interaction, which has not been evidenced in the corresponding crystallographic structure. It is interesting to compare these data to the results obtained using pose 2 as the starting conformation: Indeed, both poses share an identical orientation of the 1,2,4-triazine scaffold (Figure 5A) into the binding site, with the only difference being the orientation of the chlorophenol moiety, as highlighted in Figure S1 in the Supporting Information. Moreover, both conformations show a very similar average fluctuation profile (RMSD) inside the binding pocket (pose 1: 2.63 ± 0.96 Å; pose 2: 1.78 ± 0.53 Å). Nevertheless, the IEFs reported in Figure S1c in the Supporting Information clearly reveal that the starting orientation of the chlorine substituent is crucial to allow the ligand to establish a stable hydrogen bond interaction with His278 (7.43): In fact, the electrostatic contribution of His278 (7.43) to ligand binding, after 60 ns of MD, is more favorable for pose 1 than for pose 2.

Poses 4 and 5 apparently show strong hydrogen bond interactions with Asn253 (6.55) and His278 (7.43) (see Figure 5B). However, these interactions are not maintained during the MD simulations (Figure 5C): Indeed, the interaction with His278 (7.43) is readily lost and the one involving Asn253 (6.55) weakens progressively. The other conformations show either weaker (poses 8 and 9) or nonexistent (poses 3, 6, 7, and 10) interactions with Asn253 (6.55) and none with His278 (7.43). The only predicted strong interaction is the hydrogen bond between pose 8 and Glu169 (EL2). In all the cases, however, the MD simulations revealed high ligand fluctuations and overall unstable interaction patterns with the only constant interaction being the hydrophobic contact with Phe168 (EL2).

The strong and stable ligand–receptor interaction pattern described for pose 1 is confirmed by the high slope coefficients values of the linear function $f(x) = m \cdot x$, fitted on the DSF data obtained from MD trajectories, reported in Table S3 in the Supporting Information.

These results confirm how difficult it might be to select a proper conformation by taking into account either only the docking score or simply the presence/absence of ligand–receptor contacts. Indeed, our MD simulations have shown that conformations initially sharing similar interaction patterns (e.g.,

dx.doi.org/10.1021/ci400532b | J. Chem. Inf. Model. 2014, 54, 169–183

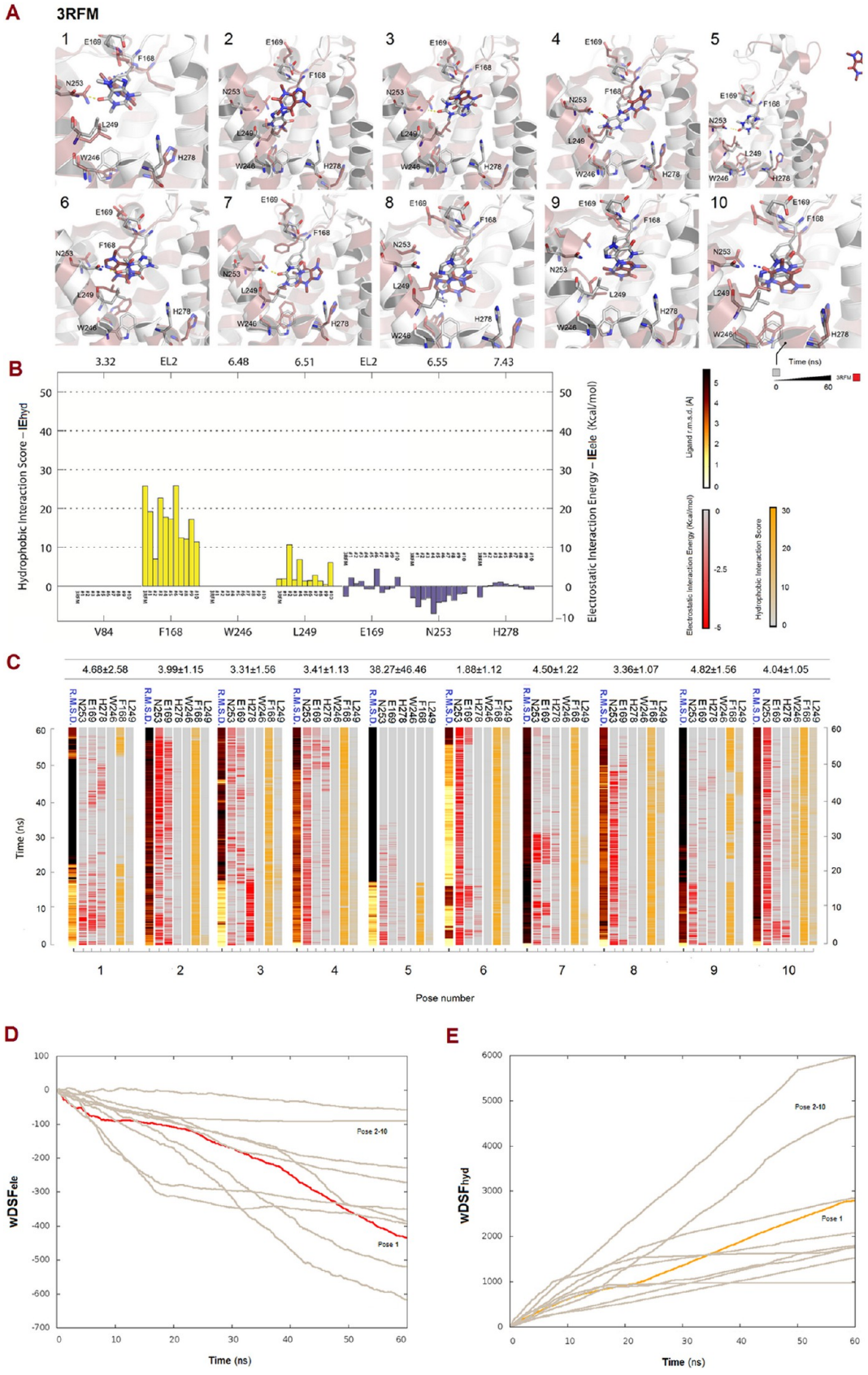

Figure 6. (A) Docking poses of caffeine at the hA_{2A} AR with their corresponding (B) static IEFs and (C) dynamic IEFs, and (D) electrostatic and (E) hydrophobic wDSFs. IE_{ele} values are given in kcal $Å^{-1}$ mol^{-1}, IE_{hyd} values are given in arbitrary hydrophobic units, and ligand fluctuations (average RMSD reported on top of the IEFs) are given in Å.

dx.doi.org/10.1021/ci400532b | J. Chem. Inf. Model. 2014, 54, 169−183

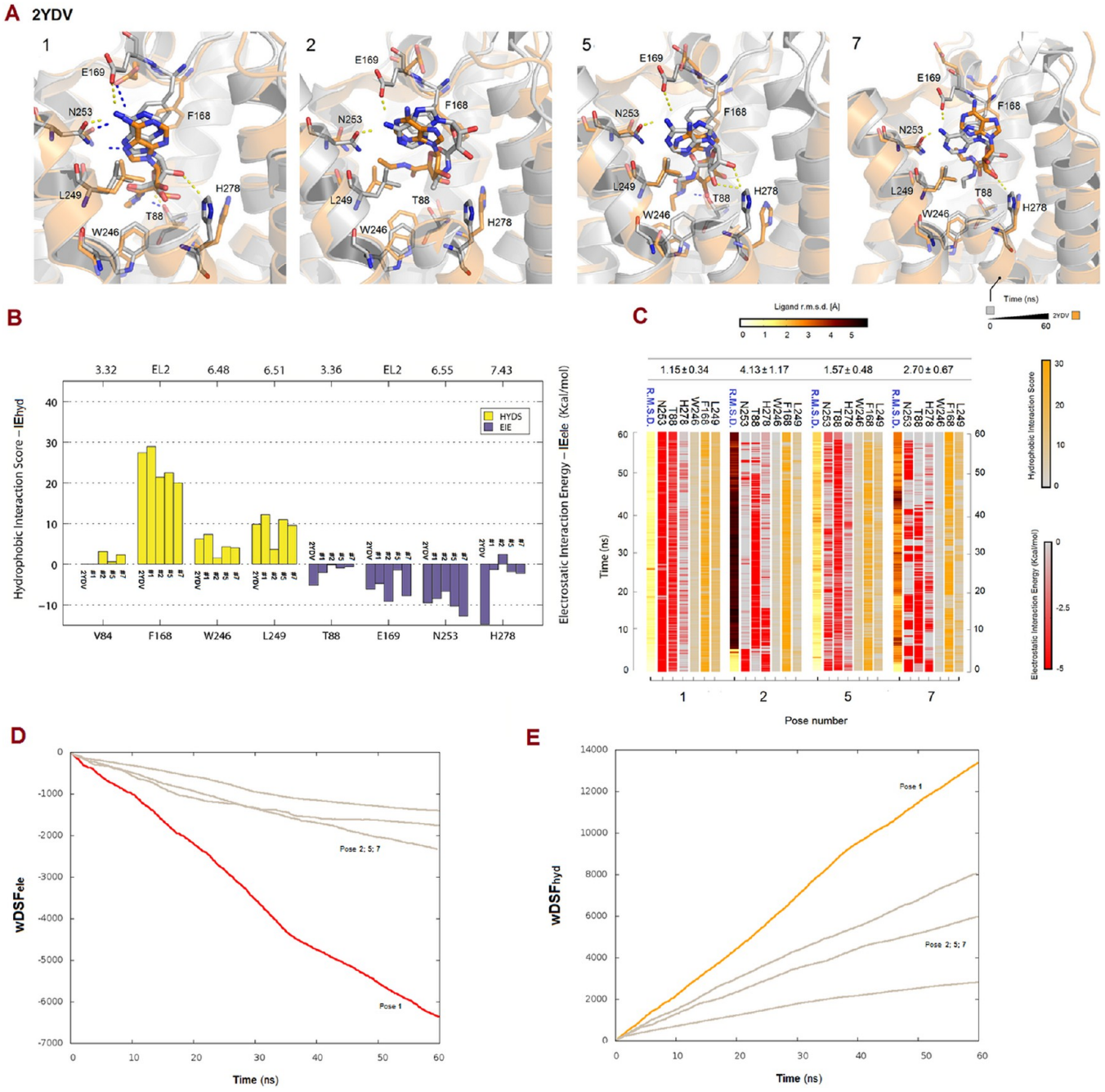

Figure 7. (A) Docking poses of NECA at the hA_{2A} AR with their corresponding (B) static IEFs and (C) dynamic IEFs, and (D) electrostatic and (E) hydrophobic wDSFs. IE_{ele} values are given in kcal $Å^{-1}$ mol^{-1}, IE_{hyd} values are given in arbitrary hydrophobic units, and ligand fluctuations (average RMSD reported on top of the IEFs) are given in Å.

pose 1 and pose 2) may temporally evolve in final states exhibiting different ligand−receptor interactions. This further emphasizes the importance of selecting a proper binding mode, especially in all those cases where no crystal structures are available for comparison (e.g., when the target structure has not yet been solved and one relies on homology models). So, we believe that, in these cases, our proposed protocol might help in selecting the binding mode: In fact, we have recently applied the combined methodology to discern between two possible binding modes of a series of 5-alkylaminopyrazolo[4,3-*e*]1,2,4-triazolo[1,5-*c*]pyrimidine at the hA_3 AR.[53] In that specific case, the MD simulations have helped in supporting a binding mode that was apparently less plausible than the alternative one.

In Silico Inspection of Caffeine Binding Mode. The clustered binding modes of caffeine are very diversified in terms of orientation of the xanthine core, as reported in Figure 6A. However, this variability is not reflected by the calculated docking scores, which do not differentiate the crystallographic conformation (pose 1, RMSD = 0.74 Å) from the others (see Table S1 in the Supporting Information). The calculated IEFs for the retained conformations (Figure 6B) reveal also a lower amount of interactions with key residues, with respect to the aforementioned cases, with the only significant interactions being a hydrogen bond with Asn253 (6.55) and the hydrophobic contacts occurring with the Phe168 (EL2) side chain. This unstable interaction network is further confirmed by

dx.doi.org/10.1021/ci400532b | J. Chem. Inf. Model. 2014, 54, 169−183

the analysis of the dynamic IEFs (Figure 6C), the ligand positional stability profiles and the collected DSF data (see Figures 6D and 6E and Table S3 in the Supporting Information). These results highlight that it is a difficult task to reproduce the "bioactive" conformation of low affinity ligands showing fragment-like features and lacking strong interactions with the binding site, as, in these cases, there are no energy criteria that can guide the selection of a proper binding mode.

In Silico Inspection of NECA Binding Mode. Four possible binding modes of NECA were retained on the basis of the possible orientations of the adenine ring inside the hA_{2A} AR orthosteric binding pocket (see Figure 7A). Selected poses have RMSD values, with respect to the crystallographic structure, that span from 0.29 Å (pose 1, Table S1 in the Supporting Information) to 4.98 Å (pose 2, Table S1 in the Supporting Information).

Pose 1 (Figure 7A) interacts with residues that hold a crucial role in agonist and antagonist recognition. The side chains of Asn253 (6.55) and Glu169 (EL2) residues establish hydrogen bonds with the exocyclic nitrogen atom of the purine nucleoside derivative. The aromatic purine core, which additionally interacts with Leu249 (6.51), is involved in a $\pi-\pi$ stacking interaction with the conserved Phe168 (EL2) side chain. The ribose moiety, which is deeply inserted in the orthosteric binding pocket, interacts with Thr88 (3.36) and His278 (7.43) through a network of hydrogen bond interactions. During the MD simulation (Figure 7C), the polar contacts with Asn253 (6.55), Glu169 (EL2), and Thr88 (3.36) are maintained strong and persistent, whereas the favorable interaction with His278 (7.43), which is initially involved in a strong interaction with the ligand (Figure 7B), is lost during the simulation. However, the interactions between His278 (7.43) and the ligand are mediated by water molecules, as discussed in the paragraph below.

The dynamic IEFs (Figure 7C) highlight persistent hydrophobic contacts with Leu249 (6.51), Phe168 (EL2) and Trp246 (6.48). The stability of the initial binding mode is also confirmed by the low ligand fluctuation (average RMSD = 1.150 ± 0.34 Å), higher slope coefficients (Table S3 in the Supporting Information) associated with the DSFs (Figures 7D and 7E). The other predicted binding conformations establish hydrogen bond interactions with the Asn253 (6.55) and Glu169 (EL2) side chains (figure 7b). In all these cases, the MD simulations (Figure 7C) have revealed unstable interaction patterns and a lower positional stability, with respect to pose 1, with an increase of the ligand fluctuations into the binding site.

Therefore, despite the fact that different conformations might present similar interaction patterns with residues that play a key role in antagonist or agonist recognition at the hA_{2A} AR (Figure 4B), a "post-processing" selection of the docked poses based on either the docking score or simple visual inspection could lead to misleading results and even failures when building SAR reports. Instead, our proposed analysis of dynamic IEFs, ligand positional stability (RMSD profile), and DSFs has proven to be able to discern the "bioactive" binding mode among other conformations. Indeed, our analysis has highlighted that the conformation with the highest degree of fitness to the hA_{2A} AR binding pocket (which is the one closest to the crystallographic structure) presents a less marked average fluctuation with respect to the other sampled conformations and both stable polar interactions and persistent hydrophobic contacts. The latter aspects could be better understood by analyzing the slope coefficients of the trend line fitted on the DSF data. The conformations that possess an high degree of fitness inside the hA_{2A} AR orthosteric binding pocket are most likely to be characterized by higher slope coefficients (absolute values). These values highlight that strong interactions with crucial residues are maintained through all MD trajectory, thus steadily increasing the cumulative sum of electrostatic interaction energies or hydrophobic score.

In Silico Inspection of Water Molecules Clusters. As previously stated, the scoring functions often fail to properly predict binding affinities, because of their limited description of protein flexibility and the implicit treatment of the solvent. The fully atomistic MD protocol has the advantage to explore along with the hA_{2A} AR−ligand complex flexibility also its dynamical solvation process, thus by providing useful insights into the role of water molecules in the ligand−protein recognition mechanism. The possible structural presence of ordered clusters of water molecules in the proximity of highly conserved motifs in class A GPCRs has been already deeply discussed in the past years[54] and recently clarified for the hA_{2A} AR.[55] Therefore, for each considered ligand−protein complex, we monitored the permanency of water molecules within three different regions, defined as extracellular cluster (EC), central cluster (CC), and intracellular cluster (IC). Here, we describe the EC, whereas descriptions of the CC and IC can be found in the Supporting Information.

The extracellular (EC) cluster (see the left central panel in Figure S3 in the Supporting Information) is located inside the orthosteric binding pocket and plays a crucial role in ligand binding. Hence, we inspected the presence and permanence through the simulation time of unique water molecules within a range of 3.6 Å (donor/acceptor distance) from ligand potential donor or acceptor atoms. In the case of ZM 241385 (PDB ID: 3EML),[15] the presence of a cluster of water molecules plays a role in bridging the ligand to TM2 and TM7 (see Figure S3 in the Supporting Information, upper panel): In particular, TIP161 and TIP6978 (15% permanency) are part of an organized cluster that bridges His278 (7.43) to the nitrogen atom of the triazolotriazine. This might account for the role of His278 (7.43) in the antagonists binding revealed by mutagenesis data,[56] but that has not been yet reported for ZM 241385, although, in recent X-ray structures,[15,55] two water molecules have been observed between the ligand aromatic core and the His278 (7.43) side chain. In the case of NECA (PDB ID: 2YDV[17]), we found the presence of a similar organized cluster of water molecules (TIP1706, TIP3138, and TIP2418) that connects TM7 to the ligand. The dynamic evolution the binding mode of T4G has also highlighted the presence of a water molecule (in rapid exchange) that bridges His278 (7.43) to the nitrogen atom of the 2,6-dimethylpyridin-4-yl substituent (see the upper panel in Figure S3b in the Supporting Information). Water molecules that establish hydrogen bonds with the 1,2,4-triazin-3-amine core have been detected also within a range of 4 Å around T4E, but they are in rapid exchange with other solvation molecules (permanence time <2%). The analysis of the evolution of caffeine binding mode has instead revealed a greater number of water molecules in rapid exchange around the antagonist structure: This is a direct consequence of the weak interactions that the ligand establishes with the protein residues, which make the structure more likely to be surrounded by solvent molecules.

In Silico Inspection of Protein Stability. In addition to the above-described analyses, the overall biophysical stability of

dx.doi.org/10.1021/ci400532b | J. Chem. Inf. Model. 2014, 54, 169−183

the solvated protein−membrane systems has been also assessed. We analyzed in details the conformational stability of each ligand−protein complex by evaluating the fluctuations of the α carbon atoms during the MD simulations. The results reported in Figure S4 in the Supporting Information highlight a common flexibility pattern among all complexes: In particular, transmembrane domains are relatively stable at their starting position (RMSD < 2 Å), whereas intracellular and extracellular loops present a higher flexibility.

CONCLUSIONS

In the present work, we have presented a combined strategy based on the integration of molecular docking and membrane molecular dynamics (MD) simulations. The main aim of our approach has been to merge the rapid sampling of ligand poses into in the binding site—distinctive of docking algorithms—with the thermodynamic accuracy of MD simulations in describing, at the molecular level, the stability of a G protein-coupled receptor (GPCR)−ligand complex embedded into a explicit lipid−water environment.

We selected, as a test case, the human A2A adenosine receptor (hA_{2A} AR) in complex with four antagonists—namely, ZM 241385, T4G, T4E, and caffeine—and one agonist (*N*-ethyl-5′-carboxamido adenosine, NECA), and evaluated the ability of our strategy in reproducing their "bioactive" conformation and in discerning it from other poses generated by the docking protocol. Once a proper conformation has been selected, we evaluated the temporal evolution of the occurring ligand−receptor interactions by introducing the concept of "dynamic IEFs" (where the term "IEFs" represents interaction energy fingerprints).

The above-described results have shown that our post-processing procedure can be regarded as a valuable alternative of conventional scoring functions, as it is able to discern/anticipate the "bioactive" conformation of high affinity ligands and to take into account both the complex flexibility in the membrane environment as well as water-driven interactions, which are two aspects of the binding that docking protocols are not yet able to handle with satisfying accuracy. In addition, our proposed strategy might represent a tool to detect and validate the feasibility of alternative binding conformations, as proposed by the docking algorithm: In this case, indeed, a scoring function-driven selection of the poses might mislead, as highlighted by several examples above-discussed.

We also believe that the proposed strategy can be extended to other GPCRs, as well as to homology models. In the latter case, the selection of a proper binding mode is a difficult task, because of the lack of a reference crystal structure. In such perspective, the analysis of dynamic IEFs and of ligand fluctuation profiles as well as the introduction of a "dynamic scoring function", provided by our combined approach, might represent a valuable help in the choice and represent a valuable tool to generate accurate models of GPCRs in complex with their ligands. In such perspective, we recently applied the herein proposed protocol during the GPCR Structure-Based Homology Modeling and Docking Assessment 2013 (http://gpcr.scripps.edu/GPCRDock2013)[57] and demonstrated how the methodology substantially improves the quality of GPCRs homology models, in terms of ligand−receptor contacts. Therefore, we strongly believe that the proposed protocol might represent an efficient method to improve the quality of homology models for docking and screening applications, with the only crucial requirements being the availability of a high-quality receptor model and a high degree of certainty of residues involved in binding.

ASSOCIATED CONTENT

Supporting Information

Tables summarizing data on the retained docked poses (Table S1), biophysical stability of membrane-embedded ligand-protein systems (Table S2), slope coefficients of linear functions fitted on DSF data (Table S3), supplementary figures (Figures S1−S4), and videos (Videos S1−S5). This material is available free of charge via the Internet at http://pubs.acs.org

AUTHOR INFORMATION

Corresponding Author

*Tel.: +39 049 8275704. Fax: +39 049 827 5366. E-mail: stefano.moro@unipd.it.

Notes

The authors declare no competing financial interest.

ACKNOWLEDGMENTS

The molecular modeling work coordinated by S.M. has been carried out with financial support of the University of Padova, Italy, and the Italian Ministry for University and Research (MIUR), Rome, Italy. S.M. is also very grateful to Chemical Computing Group and Acellera, Ltd., for the scientific and technical partnership.

ABBREVIATIONS

ARs = adenosine receptors; DSF = dynamic scoring function; EL2 = second extracellular loop; GPCRs = G protein-coupled receptors; GPU = graphics processing unit; IEFs = interaction energy fingerprints; MD: molecular dynamics; n.d. = not determined; NECA = *N*-ethyl-5′-carboxamido adenosine; POPC = 1-palmitoyl-2-oleoyl-sn-glycero-3-phosphocholine; T4E = 4-(3-amino-5-phenyl-1,2,4-triazin-6-yl)-2-chlorophenol; T4G = 6-(2,6-dimethylpyridin-4-yl)-5-phenyl-1,2,4-triazin-3-amine; TM = transmembrane; ZM 241385 = 4-(2-(7-amino-2-(2-furyl)(1,2,4)triazolo(2,3-*a*)(1,3,5)triazin-5-yl-amino)-ethyl)phenol

REFERENCES

(1) Pierce, K. L.; Premont, R. T.; Lefkowitz, R. J. Seven-transmembrane receptors. *Nat. Rev. Mol. Cell Biol.* **2002**, *3*, 639−650.
(2) Sodhi, A.; Montaner, S.; Gutkind, J. S. Viral hijacking of G-protein-coupled-receptor signalling networks. *Nat. Rev. Mol. Cell Biol.* **2004**, *5*, 998−1012.
(3) Kristiansen, K. Molecular mechanisms of ligand binding, signaling, and regulation within the superfamily of G-protein-coupled receptors: Molecular modeling and mutagenesis approaches to receptor structure and function. *Pharmacol. Ther.* **2004**, *103*, 21−80.
(4) Drews, J. Drug discovery: A historical perspective. *Science* **2000**, *287*, 1960−1964.
(5) Hopkins, A. L.; Groom, C. R. The druggable genome. *Nat. Rev. Drug Discovery* **2002**, *1*, 727−730.
(6) Jacobson, K. A.; Costanzi, S. New insights for drug design from the X-ray crystallographic structures of G-protein-coupled receptors. *Mol. Pharmacol.* **2012**, *82*, 361−371.
(7) Warren, G. L.; Andrews, C. W.; Capelli, A.-M.; Clarke, B.; LaLonde, J.; Lambert, M. H.; Lindvall, M.; Nevins, N.; Semus, S. F.; Senger, S.; Tedesco, G.; Wall, I. D.; Woolven, J. M.; Peishoff, C. E.; Head, M. S. A critical assessment of docking programs and scoring functions. *J. Med. Chem.* **2006**, *49*, 5912−5931.
(8) Böhm, H.-J.; Stahl, M. The Use of Scoring Functions in Drug Discovery Applications. In *Reviews in Computational Chemistry*;

Lipkowitz, K. B., Boyd, D. B., Eds.; John Wiley & Sons, Inc.: New York, 2003; pp 41−87.
(9) Dror, R. O.; Pan, A. C.; Arlow, D. H.; Borhani, D. W.; Maragakis, P.; Shan, Y.; Xu, H.; Shaw, D. E. Pathway and mechanism of drug binding to G-protein-coupled receptors. *Proc. Natl. Acad. Sci. U.S.A.* **2011**, *108*, 13118−13123.
(10) Dror, R. O.; Jensen, M. Ø.; Borhani, D. W.; Shaw, D. E. Exploring atomic resolution physiology on a femtosecond to millisecond timescale using molecular dynamics simulations. *J. Gen. Physiol.* **2010**, *135*, 555−562.
(11) Buch, I.; Harvey, M. J.; Giorgino, T.; Anderson, D. P.; De Fabritiis, G. High-throughput all-atom molecular dynamics simulations using distributed computing. *J. Chem. Inf. Model.* **2010**, *50*, 397−403.
(12) Harvey, M. J.; Giupponi, G.; Fabritiis, G. D. ACEMD: Accelerating Biomolecular Dynamics in the Microsecond Time Scale. *J. Chem. Theory Comput.* **2009**, *5*, 1632−1639.
(13) Haskó, G.; Linden, J.; Cronstein, B.; Pacher, P. Adenosine receptors: Therapeutic aspects for inflammatory and immune diseases. *Nat. Rev. Drug Discovery* **2008**, *7*, 759−770.
(14) Doré, A. S.; Robertson, N.; Errey, J. C.; Ng, I.; Hollenstein, K.; Tehan, B.; Hurrell, E.; Bennett, K.; Congreve, M.; Magnani, F.; Tate, C. G.; Weir, M.; Marshall, F. H. Structure of the adenosine A(2A) receptor in complex with ZM241385 and the xanthines XAC and caffeine. *Structure* **2011**, *19*, 1283−1293.
(15) Jaakola, V.-P.; Griffith, M. T.; Hanson, M. A.; Cherezov, V.; Chien, E. Y. T.; Lane, J. R.; Ijzerman, A. P.; Stevens, R. C. The 2.6 angstrom crystal structure of a human A2A adenosine receptor bound to an antagonist. *Science* **2008**, *322*, 1211−1217.
(16) Congreve, M.; Andrews, S. P.; Doré, A. S.; Hollenstein, K.; Hurrell, E.; Langmead, C. J.; Mason, J. S.; Ng, I. W.; Tehan, B.; Zhukov, A.; Weir, M.; Marshall, F. H. Discovery of 1,2,4-triazine derivatives as adenosine A(2A) antagonists using structure based drug design. *J. Med. Chem.* **2012**, *55*, 1898−1903.
(17) Lebon, G.; Warne, T.; Edwards, P. C.; Bennett, K.; Langmead, C. J.; Leslie, A. G. W.; Tate, C. G. Agonist-bound adenosine A2A receptor structures reveal common features of GPCR activation. *Nature* **2011**, *474*, 521−525.
(18) *Acellera*; http://www.acellera.com/ (accessed Jan 2, 2014).
(19) Ballesteros, J. A.; Weinstein, H. Integrated methods for the construction of three dimensional models and computational probing of structure-function relationships in G-protein coupled receptors. *Methods Neurosci.* **1995**, *25*, 366−428.
(20) Berman, H. M.; Westbrook, J.; Feng, Z.; Gilliland, G.; Bhat, T. N.; Weissig, H.; Shindyalov, I. N.; Bourne, P. E. The Protein Data Bank. *Nucleic Acids Res.* **2000**, *28*, 235−242.
(21) The Universal Protein Resource (UniProt) in 2010. *Nucleic Acids Res.* **2010**, *38*, D142−D148.
(22) Jain, E.; Bairoch, A.; Duvaud, S.; Phan, I.; Redaschi, N.; Suzek, B. E.; Martin, M. J.; McGarvey, P.; Gasteiger, E. Infrastructure for the life sciences: Design and implementation of the UniProt website. *BMC Bioinf.* **2009**, *10*, 136.
(23) Altschul, S. F.; Madden, T. L.; Schäffer, A. A.; Zhang, J.; Zhang, Z.; Miller, W.; Lipman, D. J. Gapped BLAST and PSI-BLAST: A new generation of protein database search programs. *Nucleic Acids Res.* **1997**, *25*, 3389−3402.
(24) Labute, P. Protonate3D: Assignment of ionization states and hydrogen coordinates to macromolecular structures. *Proteins* **2009**, *75*, 187−205.
(25) Wang, J.; Cieplak, P.; Kollman, P. A. How well does a restrained electrostatic potential (RESP) model perform in calculating conformational energies of organic and biological molecules? *J. Comput. Chem.* **2000**, *21*, 1049−1074.
(26) *Molecular Operating Environment*; http://www.chemcomp.com/ (accessed Jan 2, 2014).
(27) Stewart, J. J. P. Optimization of parameters for semiempirical methods. I. Method. *J. Comput. Chem.* **1989**, *10*, 209−220.
(28) Stewart, J. J. P. Optimization of parameters for semiempirical methods. II. Applications. *J. Comput. Chem.* **1989**, *10*, 221−264.
(29) Jones, G.; Willett, P.; Glen, R. C.; Leach, A. R.; Taylor, R. Development and validation of a genetic algorithm for flexible docking. *J. Mol. Biol.* **1997**, *267*, 727−748.
(30) Jones, G.; Willett, P.; Glen, R. C. Molecular recognition of receptor sites using a genetic algorithm with a description of desolvation. *J. Mol. Biol.* **1995**, *245*, 43−53.
(31) Dowling, J. E.; Vessels, J. T.; Haque, S.; Chang, H. X.; Van Vloten, K.; Kumaravel, G.; Engber, T.; Jin, X.; Phadke, D.; Wang, J.; Ayyub, E.; Petter, R. C. Synthesis of [1,2,4]triazolo[1,5-a]pyrazines as adenosine A2A receptor antagonists. *Bioorg. Med. Chem. Lett.* **2005**, *15*, 4809−4813.
(32) Federico, S.; Paoletta, S.; Cheong, S. L.; Pastorin, G.; Cacciari, B.; Stragliotto, S.; Klotz, K. N.; Siegel, J.; Gao, Z. G.; Jacobson, K. A.; Moro, S.; Spalluto, G. Synthesis and Biological Evaluation of a New Series of 1,2,4-Triazolo[1,5-*a*]-1,3,5-triazines as Human A_{2A} Adenosine Receptor Antagonists with Improved Water Solubility. *J. Med. Chem.* **2011**, *54*, 877−89.
(33) MacKerell, A. D., Jr.; Banavali, N.; Foloppe, N. Development and current status of the CHARMM force field for nucleic acids. *Biopolymers* **2000**, *56*, 257−265.
(34) Lomize, M. A.; Lomize, A. L.; Pogozheva, I. D.; Mosberg, H. I. OPM: Orientations of proteins in membranes database. *Bioinformatics* **2006**, *22*, 623−625.
(35) Sommer, B. Membrane Packing Problems: A Short Review on Computational Membrane Modeling Methods and Tools. *Comput. Struct. Biotechnol. J.* **2013**, *5*.
(36) Humphrey, W.; Dalke, A.; Schulten, K. VMD: Visual molecular dynamics. *J. Mol. Graphics* **1996**, *14* (33−38), 27−28.
(37) Jorgensen, W. L.; Chandrasekhar, J.; Madura, J. D.; Impey, R. W.; Klein, M. L. Comparison of simple potential functions for simulating liquid water. *J. Chem. Phys.* **1983**, *79*, 926−935.
(38) Grubmüller, H.; GrollV. *Solvate*; http://www.mpibpc.mpg.de/home/grubmueller/downloads/solvate/index.html (accessed Jan 2, 2014).
(39) Vanommeslaeghe, K.; Hatcher, E.; Acharya, C.; Kundu, S.; Zhong, S.; Shim, J.; Darian, E.; Guvench, O.; Lopes, P.; Vorobyov, I.; Mackerell, A. D., Jr CHARMM general force field: A force field for drug-like molecules compatible with the CHARMM all-atom additive biological force fields. *J. Comput. Chem.* **2010**, *31*, 671−690.
(40) Vanommeslaeghe, K.; MacKerell, A. D. Automation of the CHARMM General Force Field (CGenFF) I: Bond Perception and Atom Typing. *J. Chem. Inf. Model.* **2012**, *52*, 3144−3154.
(41) Vanommeslaeghe, K.; Raman, E. P.; MacKerell, A. D. Automation of the CHARMM General Force Field (CGenFF) II: Assignment of Bonded Parameters and Partial Atomic Charges. *J. Chem. Inf. Model.* **2012**, *52*, 3155−3168.
(42) Head-Gordon, M.; Pople, J. A.; Frisch, M. J. MP2 energy evaluation by direct methods. *Chem. Phys. Lett.* **1988**, *153*, 503−506.
(43) Frisch, M. J.; Trucks, G. W.; Schlegel, H. B.; Scuseria, G. E.; Robb, M. A.; Cheeseman, J. R.; Scalmani, G.; Barone, V.; Mennucci, B.; Petersson, G. A.; Nakatsuji, H.; Caricato, M.; Li, X.; Hratchian, H. P.; Izmaylov, A. F.; Bloino, J.; Zheng, G.; Sonnenberg, J. L.; Hada, M.; Ehara, M.; Toyota, K.; Fukuda, R.; Hasegawa, J.; Ishida, M.; Nakajima, T.; Honda, Y.; Kitao, O.; Nakai, H.; Vreven, T.; Montgomery, J. A., Jr.; Peralta, J. E.; Ogliaro, F.; Bearpark, M.; Heyd, J. J.; Brothers, E.; Kudin, K. N.; Staroverov, V. N.; Kobayashi, R.; Normand, J.; Raghavachari, K.; Rendell, A.; Burant, J. C.; Iyengar, S. S.; Tomasi, J.; Cossi, M.; Rega, N.; Millam, N. J.; Klene, M.; Knox, J. E.; Cross, J. B.; Bakken, V.; Adamo, C.; Jaramillo, J.; Gomperts, R.; Stratmann, R. E.; Yazyev, O.; Austin, A. J.; Cammi, R.; Pomelli, C.; Ochterski, J. W.; Martin, R. L.; Morokuma, K.; Zakrzewski, V. G.; Voth, G. A.; Salvador, P.; Dannenberg, J. J.; Dapprich, S.; Daniels, A. D.; Farkas, Ö.; Foresman, J. B.; Ortiz, J. V.; Cioslowski, J.; Fox, D. J. Gaussian 09, Revision B.01; Gaussian, Inc.: Wallingford, CT, 2009.
(44) Kräutler, V.; Van Gunsteren, W. F.; Hünenberger, P. H. A fast SHAKE algorithm to solve distance constraint equations for small molecules in molecular dynamics simulations. *J. Comput. Chem.* **2001**, *22*, 501−508.

(45) Allen, W. J.; Lemkul, J. A.; Bevan, D. R. GridMAT-MD: A grid-based membrane analysis tool for use with molecular dynamics. *J. Comput. Chem.* **2009**, *30*, 1952−1958.
(46) Kucerka, N.; Tristram-Nagle, S.; Nagle, J. F. Structure of fully hydrated fluid phase lipid bilayers with monounsaturated chains. *J. Membr. Biol.* **2005**, *208*, 193−202.
(47) Essmann, U.; Perera, L.; Berkowitz, M. L.; Darden, T.; Lee, H.; Pedersen, L. G. A smooth particle mesh Ewald method. *J. Chem. Phys.* **1995**, *103*, 8577−8593.
(48) Jaakola, V.-P.; Lane, J. R.; Lin, J. Y.; Katritch, V.; Ijzerman, A. P.; Stevens, R. C. Ligand binding and subtype selectivity of the human A(2A) adenosine receptor: Identification and characterization of essential amino acid residues. *J. Biol. Chem.* **2010**, *285*, 13032−13044.
(49) Cristalli, G.; Lambertucci, C.; Marucci, G.; Volpini, R.; Dal Ben, D. A2A adenosine receptor and its modulators: Overview on a druggable GPCR and on structure-activity relationship analysis and binding requirements of agonists and antagonists. *Curr. Pharm. Des.* **2008**, *14*, 1525−1552.
(50) Guvench, O.; MacKerell, A. D., Jr. Computational evaluation of protein-small molecule binding. *Curr. Opin. Struct. Biol.* **2009**, *19*, 56−61.
(51) Jansen, J. M.; Martin, E. J. Target-biased scoring approaches and expert systems in structure-based virtual screening. *Curr. Opin. Chem. Biol.* **2004**, *8*, 359−364.
(52) Wichapong, K.; Lawson, M.; Pianwanit, S.; Kokpol, S.; Sippl, W. Postprocessing of protein-ligand docking poses using linear response MM-PB/SA: application to Wee1 kinase inhibitors. *J. Chem. Inf. Model.* **2010**, *50*, 1574−1588.
(53) Federico, S.; Ciancetta, A.; Sabbadin, D.; Paoletta, S.; Pastorin, G.; Cacciari, B.; Klotz, K. N.; Moro, S.; Spalluto, G. Exploring the Directionality of 5-Substitutions in a New Series of 5-Alkylaminopyrazolo[4,3-e]1,2,4-triazolo[1,5-c]pyrimidine as a Strategy to Design Novel Human A3 Adenosine Receptors Antagonists. *J. Med. Chem.* **2012**, *55*, 9654−9668.
(54) Pardo, L.; Deupi, X.; Dölker, N.; López-Rodríguez, M. L.; Campillo, M. The role of internal water molecules in the structure and function of the rhodopsin family of G protein-coupled receptors. *Chembiochem* **2007**, *8*, 19−24.
(55) Liu, W.; Chun, E.; Thompson, A. A.; Chubukov, P.; Xu, F.; Katritch, V.; Han, G. W.; Roth, C. B.; Heitman, L. H.; IJzerman, A. P.; Cherezov, V.; Stevens, R. C. Structural basis for allosteric regulation of GPCRs by sodium ions. *Science* **2012**, *337*, 232−236.
(56) Kim, J.; Wess, J.; Van Rhee, A. M.; Schöneberg, T.; Jacobson, K. A. Site-directed mutagenesis identifies residues involved in ligand recognition in the human A2a adenosine receptor. *J. Biol. Chem.* **1995**, *270*, 13987−13997.
(57) Kufareva, I.; Katrich, V.; GPCR Dock 2013 participants; Stevens, R. C.; Abagyan, R. Advances in GPCR modeling evaluated by the GPCR Dock 2013 Assessment: Meeting new challenges. Submitted to *Structure*.